

Twenty First Quarterly Progress Report

August 1, 2011 to October 31, 2011

Contract No. HHS-N-260-2006-00005-C

Neurophysiological Studies of Electrical Stimulation for the Vestibular Nerve

Submitted by:

James O. Phillips, Ph.D.^{1,3,4}

Steven Bierer, Ph.D.^{1,3,4}

Albert F. Fuchs, Ph.D.^{2,3,4}

Chris R.S. Kaneko, Ph.D.^{2,3}

Leo Ling, Ph.D.^{2,3}

Shawn Newlands, M.D., Ph.D.⁵

Kaibao Nie, Ph.D.^{1,4}

Jay T. Rubinstein, M.D., Ph.D.^{1,4,6}

¹ Department of Otolaryngology-HNS, University of Washington, Seattle, Washington

² Department of Physiology and Biophysics, University of Washington, Seattle, Washington

³ Washington National Primate Research Center, University of Washington, Seattle, Washington

⁴ Virginia Merrill Bloedel Hearing Research Center, University of Washington, Seattle, Washington

⁵ Department of Otolaryngology, University of Rochester, Rochester, New York

⁶ Department of Bioengineering, University of Washington, Seattle, Washington

Reporting Period: August 1, 2011 to October 31, 2011

Challenges:

1. During Quarter 21 we had a hiatus in funding for the month of August. During this time we continued testing animals, but also prepared for the termination of the study by completing several behavioral studies. We hoped that a modification to our contract would allow us to continue our study for an additional year with our remaining funds and animals. In September, we received notice that we had received such a modification. We immediately began intensive longitudinal monitoring of behavioral and physiological parameters associated with electrode viability and efficacy. We are currently monitoring constant velocity horizontal sinusoidal VOR, horizontal step VOR, and constant amplitude canal plane VOR in all of our animals on a monthly basis. We are also monitoring vECAP and electrode impedance on a weekly basis. We are performing serial ABR measurements using both clicks and tones on a monthly basis. We are also performing biweekly electrical stimulation current and frequency versus eye velocity series with each of the implanted electrodes, and recording daily fixed parameter electrical stimulation. These studies are being performed in addition to neural recording and head velocity contingent stimulation.

2. We have not yet completed fabrication of our bone anchored sensory array. We had hoped to be testing this device in Quarter 21. However, the programming and preliminary testing of the device is taking longer than anticipated. We still have the laboratory version of the device implemented on a PC computer, and we will continue to perform our experiments using this tool. We hope that full fabrication of the final device will be accomplished in Quarter 22, and we will be able to begin both bench and animal testing at that time.

Successes:

1. During quarter 21 we have reviewed the longitudinal data that we have already recorded in our animals, and have added to that data set. An interim report of this data is presented below, and had been submitted as an abstract to the annual ARVO meeting. Figure 1 displays the longitudinal changes in eye velocity elicited by a fixed parameter constant frequency and constant current stimulus delivered to the lateral canal in 6 monkeys. The parameters were selected to produce relatively robust slow phase velocities in each animal at the outset of data collection. The figure shows that three of the monkeys showed a decrease in horizontal slow phase eye velocity over time, two of the monkeys showed an increase in slow phase velocity over time, and one monkey showed no change in slow phase velocity over time. Data collection is continuing in three of the monkeys shown in this figure. These results indicate that we can maintain the viability of the prosthesis over time, but that the time course of changes in efficacy is highly variable across monkeys.

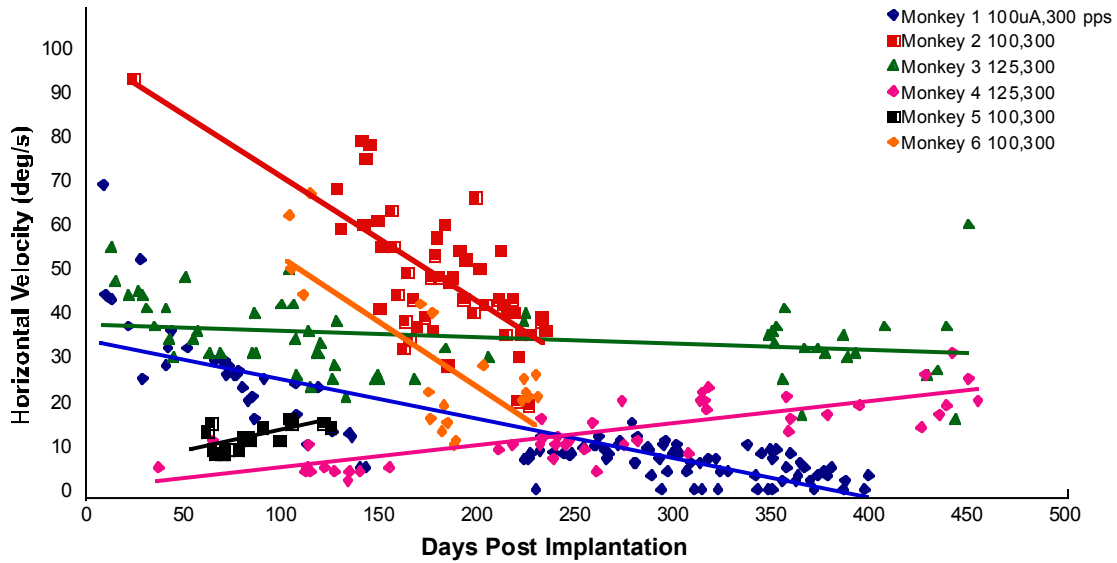


Figure 1. Average horizontal slow phase velocity versus days after implantation for 6 monkeys. Legend indicates the stimulus current and frequency for 2 s trains of biphasic pulses, 100 μ s per phase and 8 μ s interphase gap.

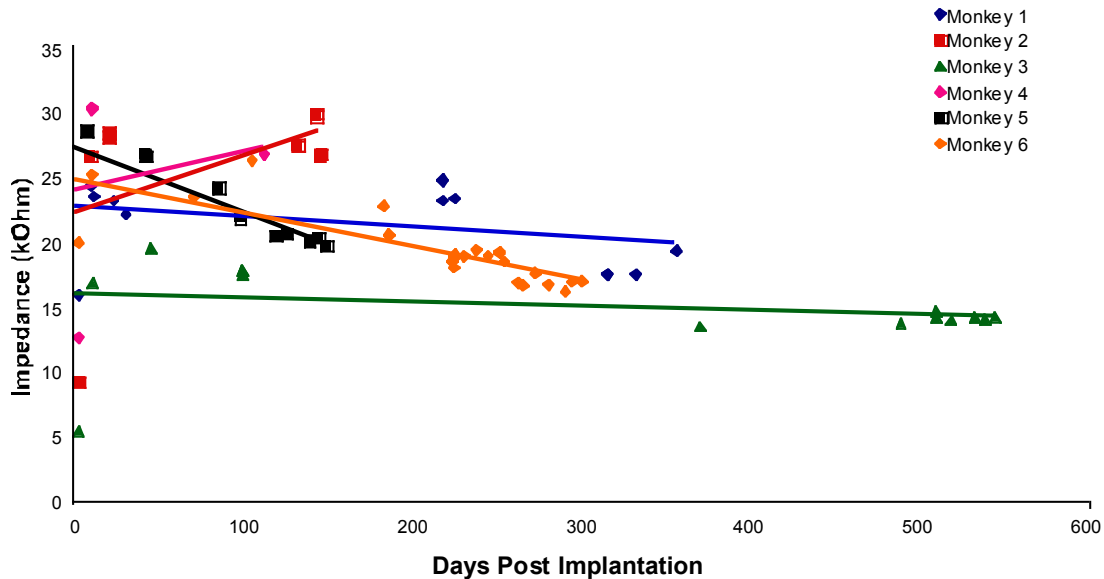


Figure 2. Impedance versus days after implantation for 6 monkeys.

We also looked to see if there was a comparable progression in the impedance of the electrodes over time. We reasoned that changes in stimulation efficacy might be related to changes in the electrodes or the tissue immediately surrounding the electrodes. Figure 2 shows changes over time in the impedance of the most distal electrode (tip electrode) of the lateral canal array in each of the animals shown in Figure 1. This was the electrode that was activated using a remote ground as the return path to produce the data displayed in Figure 1. As can be seen in the figure, there is typically little change in the electrode impedance over time. The most stable impedance was for the electrode in Monkey 3, which also showed a relatively stable stimulation efficacy over time. However, there was not a consistent relationship between electrode impedance and efficacy for the other

animals. Since the times of data collection for impedance and velocity data differ, it is difficult to draw firm conclusions from this data. Impedance data collection is continuing in three of the monkeys shown in this figure.

We also examined whether there was a relationship between changes in the efficacy of stimulation through electrodes in one canal in an animal and changes in the efficacy of stimulation through the other electrodes. In Figure 3, we examine changes in efficacy of stimulation in both the lateral and posterior canal in a single animal. The figure plots the vertical and horizontal slow phase eye velocities elicited by electrical stimulation of the posterior and horizontal canals, respectively, over time. It is clear that while the posterior canal stimulation became more effective over time, the lateral canal stimulation produced relatively similar results over time.

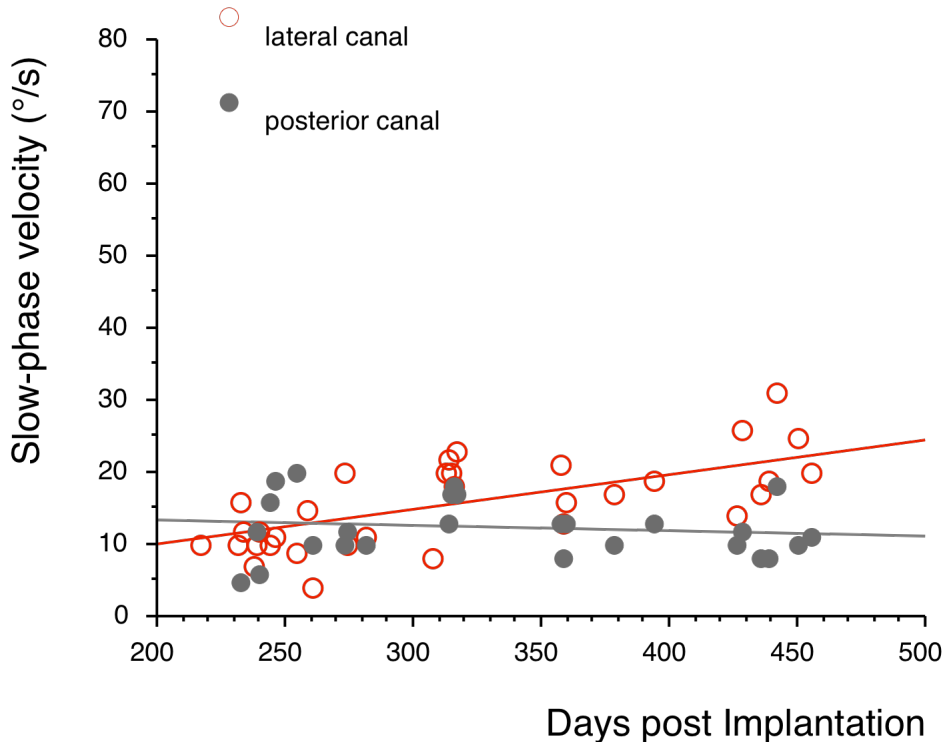


Figure 3. Slow phase velocity versus current for stimulation of the lateral and posterior canal in a single monkey versus times following implantation. Horizontal velocities are displayed for lateral canal stimulation and vertical velocities are displayed for posterior canal stimulation.

We also looked to see if there were uniform changes in the eye velocity response to single canal stimulation at different currents or different frequencies of stimulation. If the changes in efficacy of stimulation were canal independent and varied with frequency and current, this would produce a programming (mapping) nightmare for a vestibular prosthesis. The results of this analysis are shown in Figure 4. Figure 4A shows that for

three different standard currents of stimulation, there was little change in the efficacy of stimulation in this particular canal over time. Figure 4B shows that that the same is true for three standard frequencies of stimulation. This result suggests that over time, the effects of stimulation change similarly at different frequencies and currents. This result is being confirmed longitudinally in the animals that remain in our study.

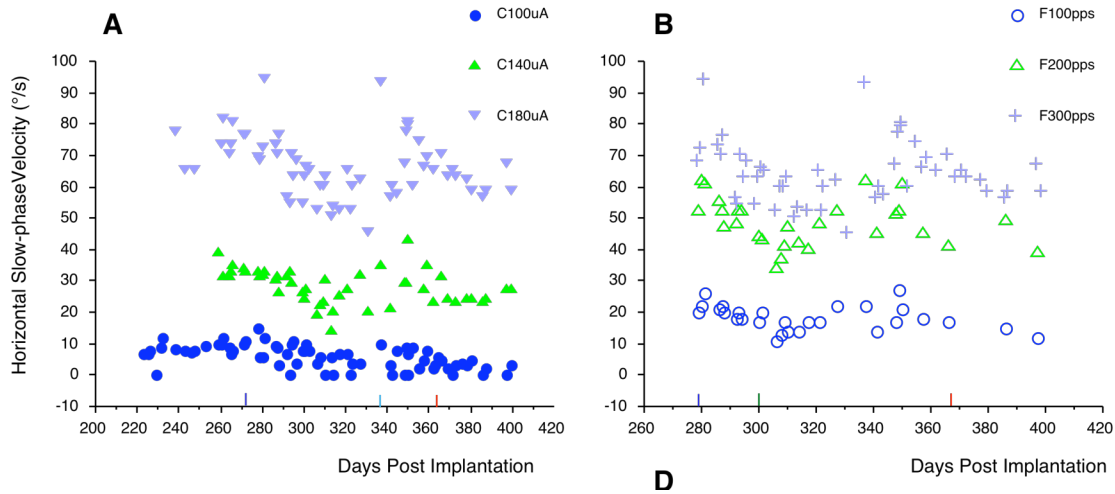


Figure 4. Changes in horizontal slow phase velocity from electrical stimulation at different frequencies and currents versus time following implantation of the lateral canal. A. Changes in slow phase velocity elicited from lateral canal stimulation at three currents. B. Changes in slow phase velocity elicited from lateral canal stimulation at three frequencies.

2. We have noted a recovery in the hearing of a monkey that underwent implantation of electrode arrays in three canals. In this animal, click thresholds remained stable at 75dB attenuation, pre-operatively, immediately post operatively, and at 5 months in the non-implanted left ear. In the implanted right ear, the pre-operative click threshold was 80 dB attenuation. Immediately post-operatively, the threshold was 57 dB attenuation, and at 5 months the click threshold had recovered to 75dB attenuation. The tone threshold at 5 months also resembled the pre-operative data at 2kHz with a threshold at approximately 85dB attenuation. The 500Hz threshold was at approximately 45dB attenuation, and the 8kHz threshold was at approximately 50dB attenuation. Overall, there was a significant improvement in ABR thresholds compared to the initial post-operative ABRs. The short term hearing loss significantly recovered in the 5 months following implantation.

3. In this quarter we moved forward on several patents related to the development of the vestibular prosthesis. The IP created through our ongoing work is listed below.

Innovation ID: 45552

Status: Project Development

Date Received: 3/13/2011

Title: Method to Decrease spontaneous firing rate of electrically stimulated nerve.

Innovation ID: 44432

Status: Marketing

Date Received: 1/4/2008

Title: Intralabyrinthine electrode array for a vestibular prosthesis.

Patent: 44432.01AU1

Status: Converted

Filing Date: 5/29/2009

Application # 2009902449

Foreign Patent

Patent: 44432.02W02

Status: Pending

Filing Date: 5/28/2010

Application # PCT/AU2010/000655

PCT Patent

Innovation ID: 44789

Status: Marketing

Date Received: 11/29/2009

Title: Vestibular implant for the treatment of Meniere's disease.

Patent: 44789.01US1

Status: Converted

Filing Date: 5/29/2009

Application # 61/182,534

US Patent

Patent: 44803.02W02

Status: Pending

Filing Date: 5/28/2010

Application # PCT/US10/36729

PCT Patent

Innovation ID: 44803

Status: Marketing

Date Received: 11/24/2009

Title: Electrically evoked compound action potentials to guide placement and programming of a vestibular neural stimulator.

Patent: 44803.01US1

Status: Converted

Filing Date: 5/29/2009

Application # 61/182,526

US Patent

Patent: 44803.02W02

Status: Pending

Filing Date: 5/28/2010

Application # PCT/US10/36729
PCT Patent

Innovation ID: 45570
Status: Project Development
Date Received: 3/28/2011
Title: Real time communication link for a vestibular prosthesis.
Patent: 45570.01US1
Status: Pending
Filing Date: 6/17/2011
Application # 61/498,117
US Patent

Innovation ID: 45116
Status: Project Development
Date Received: 12/3/2009
Title: Vestibular gain enhancement by unmodulated peripheral pacing.
Patent: 44803.02W02
Status: Pending
Filing Date: 5/28/2010
Application # PCT/US10/36729
US Patent

Innovation ID: 45568
Status: Project Development
Date Received: 3/27/2011
Title: A bone anchored sensory array/processor for a vestibular prosthesis.

4. We continued development of our bone anchored sensor array compatible with our implanted vestibular stimulator. We have completed fabrication of the sensor boards and electronics, and have finalized designs for the primate research interface internal enclosure and mounting system and the human interface internal enclosure and mounting system. The primate enclosure is being constructed currently. The designs for these elements are pictured below.

Figure 5 displays the bone anchored sensor array board design and fabricated pieces. We are using a 4 layer board (top to bottom, red, brown, green, blue). The sensor and the microcontroller are mounted on opposite faces of the board, and are oriented at 45 degrees to one another. This board is designed to lie in the horizontal plane, with the AP dimension running with the long axis of the board. This will put the sensors roughly in the plane of the semicircular canals.

The board is enclosed in a titanium housing which is designed to be covered in a plastic case. The design of the housing and attachment assembly for the primate and human device are shown in Figure 6, below. The human device is identical to the primate device except for the attachment tab, which is made to be implanted into the skull in humans and

to be incorporated into the existing acrylic stabilization lugs in non-human primates. The attachment tab is to be implanted stereotaxically with reference to the plane of the implanted canals as imaged on high resolution CT. The tab is secured to the case via a slot and pressure points (not shown) that secure the device in a fixed orientation on the skull. The external device is powered by a separate small battery pack, which is attached via a cord. The device incorporates a capacitor to allow for continued operation during battery changes.

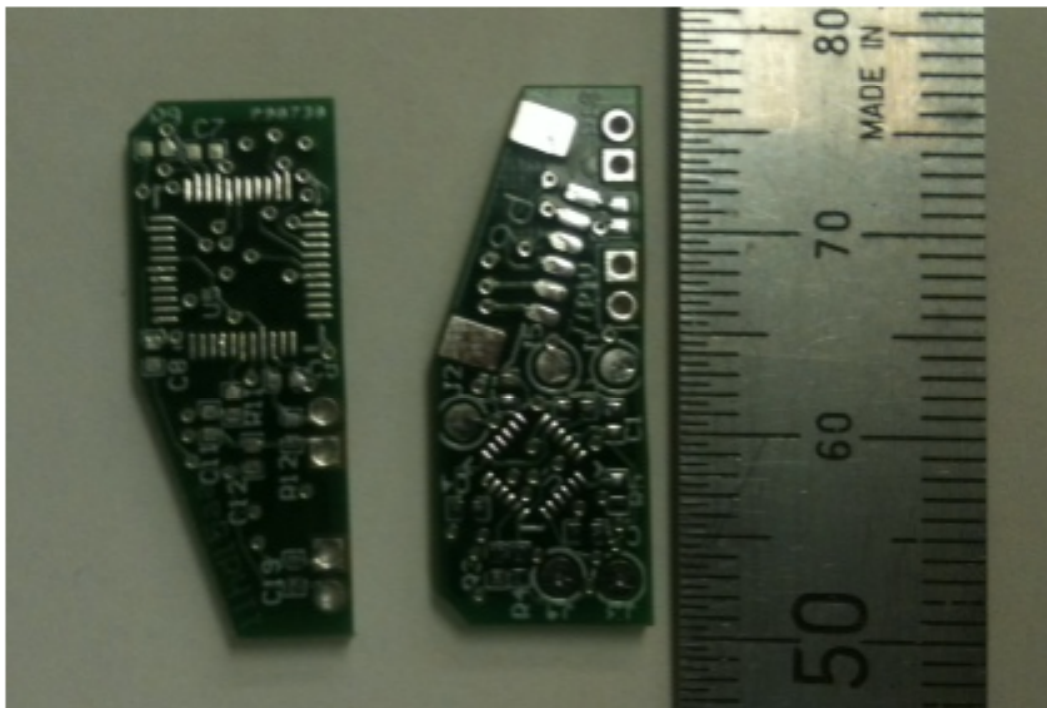
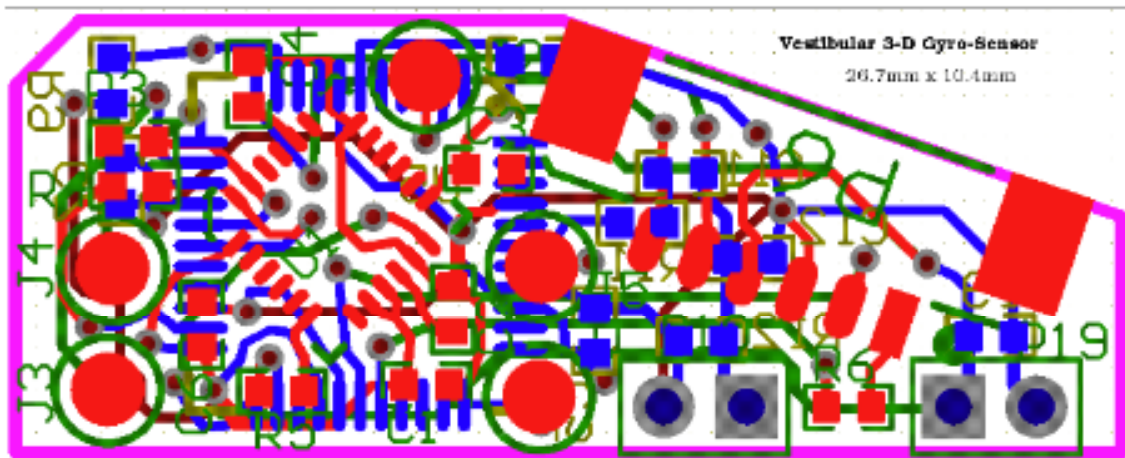


Figure 5. Bone anchored sensor array design and fabricated assembly.

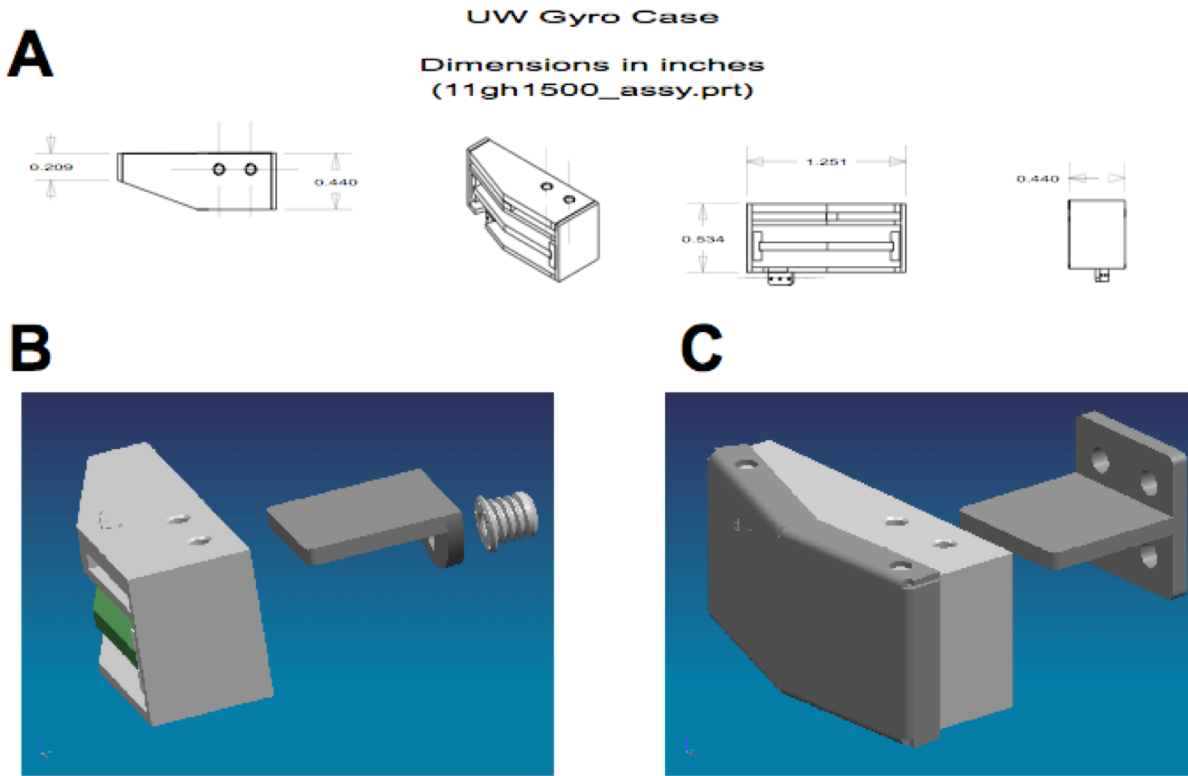


Figure 6. Bone anchored sensor array case design and configuration. A. Dimensions in inches for the titanium inner case. B. Human assembly with bone anchor, attachment fin, and open case showing electronic (green) and attachment slot. C. Non-human primate assembly showing identical case to A with cover, but screw plate and attachment fin for mounting on existing acrylic.

5. We continued to study the relationship between vestibular neuron discharge and current and frequency of electrical stimulation. We recorded from several neurons that displayed a change in timing of spike discharge with increases in stimulation current, but did not actually add spikes to their discharge in response to electrical stimulation. The electrical stimulation appeared to align spikes to the electrical stimulus, rather than adding spikes to the discharge of the recorded neurons. For other neurons a clear change in rate of firing and the number of spikes was observed.

Figure 7 shows the change in discharge for a neuron that does not add spikes with electrical stimulation. The animal is fixating a point target to eliminate any eye movement artifact that would result from activation of slow phase eye movements with the stimulation. With the onset of stimulation, the unit activity clearly aligns on the electrical stimulus, as shown in the spike histogram. However, there is no increase in the rate of discharge over the background rate, as shown in the instantaneous firing rate (IFR) trace.

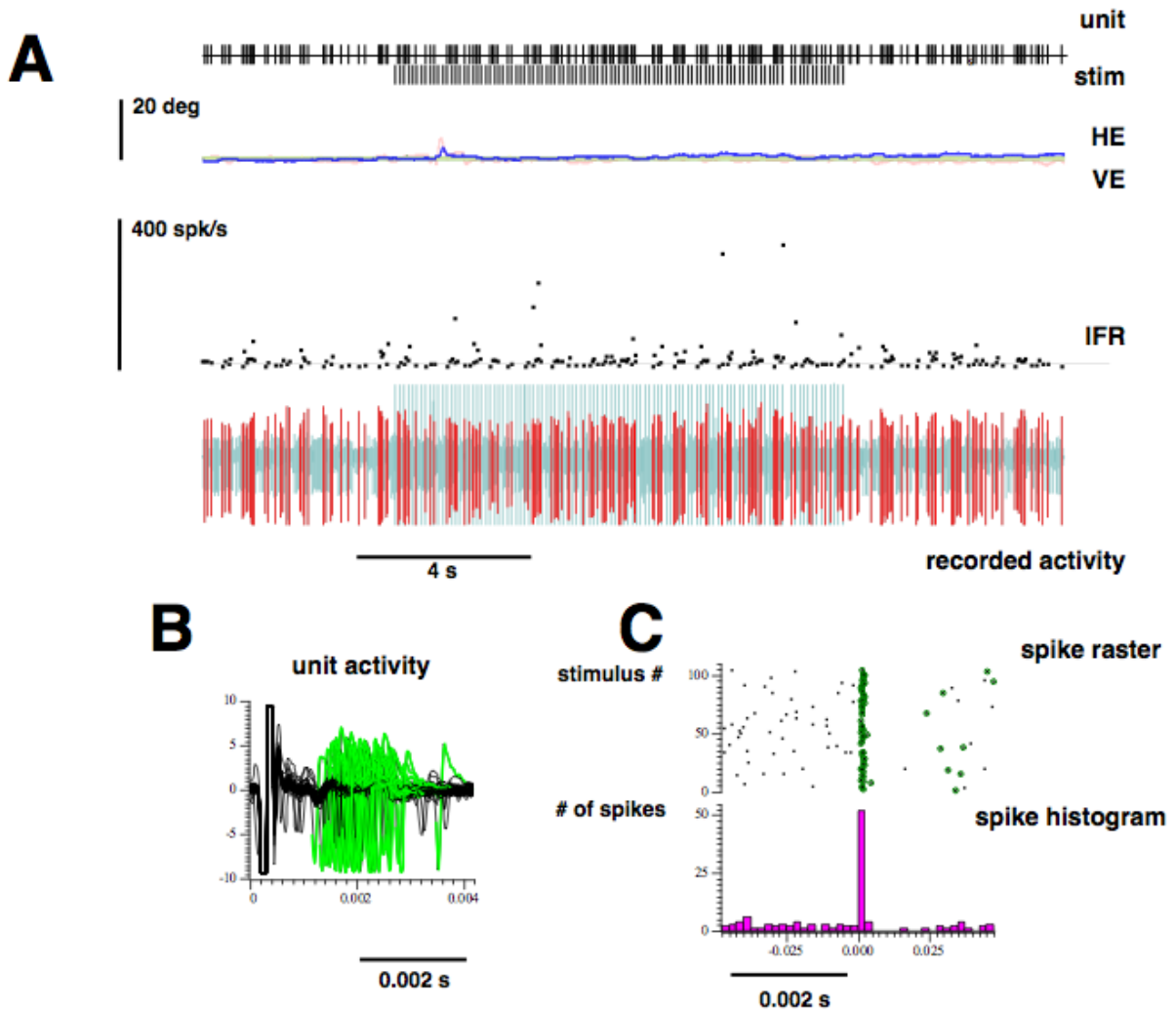


Figure 7. Discharge of a vestibular neuron during stable fixation and electrical stimulation of the lateral canal at 10pps and $180\mu\text{A}$. (A, main panel) unit, isolated discharge of the recorded neurons; stim, occurrence of the electrical stimulus; VE, vertical eye position; HE, horizontal eye position superimposed on target position re chair (stable in the world); IFR, instantaneous firing rate, recorded activity (red for neuron and grey for stimulus artifact and other neural activity in the background). (B, inset left) The unit activity in green is superimposed on the stimulus artifact in black. (C, inset right) The spike histogram is aligned on the time of the electrical stimulus. (Note: The apparent modulation in the constant stimulation rate is an artifact of the digital rendering, and is not real.)

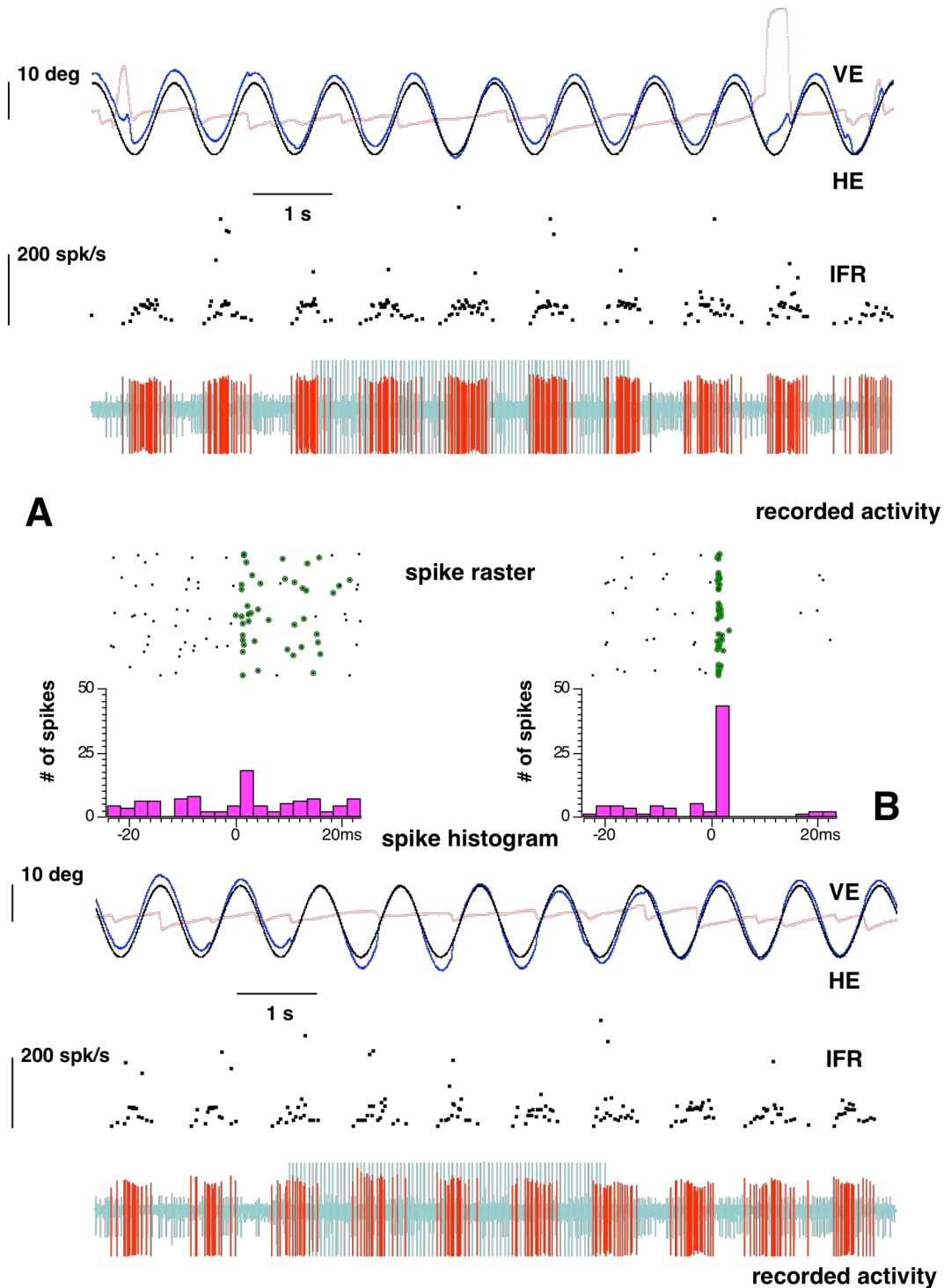


Figure 8. Discharge of a vestibular neuron during sinusoidal head rotation and electrical stimulation of the lateral canal at 20pps and 120 μ A in A, and at 20pps and 240 μ A in B. The spike histograms are aligned on the time of the electrical stimulus. VE, vertical eye position; HE, horizontal eye position superimposed on target position re chair (stable in the world); IFR, instantaneous firing rate, recorded activity (red for neuron and grey for stimulus artifact and other neural activity in the background).

Figure 8 illustrates that increases in current can change the alignment of a neuron's spikes without changing the absolute firing rate. In this example, the same neuron as displayed in Figure 7 is modulated by chair rotation and driven by lateral canal electrical stimulation at two currents. As the current increases from 120 μA to 240 μA there is a change in the timing of the neural discharge, so that the spikes become better aligned on the electrical stimulus, as seen in the spike histograms for Figure 8A (low current) and Figure 8B (higher current). However, the overall unit discharge rate and depth of modulation do not change. The neuron is still modulated by the rotation, even pausing for head movement in the off direction. Presumably, as the neuron approaches threshold for firing, the electrical stimulus drives it above threshold. At other times, when the chair is moving to the right, the neuron is too far below threshold to fire, eliminating both its tonic resting discharge and the activity that should result from the electrical stimulation.

Another way of quantifying the neural discharge in Figure 8 is to calculate the percentage of time that a spike occurs and there is a discharge of the neuron within a specified time window, in this case 0.7 ms to 2.5 ms, which is 1-2 synaptic latencies. We call this metric discharge %, or D%. For the neuron in Figure 8, the D% was 18% at 120 μA and 53% at 240 μA , which is reflected in the height of the spike histograms.

We are now calculating D% for all of our recorded neurons at different stimulation currents and frequencies. Figure 9 shows the D% for 10 neurons. In the upper panel of Figure 9, the D% is plotted as a function of stimulation current for a stimulation frequency of 20 pps. For several of the displayed neurons, especially those with low thresholds, there is a step increase in D% from threshold to a fairly constant value with increasing current. For other neurons, there is a more gradual change in D% with current. In the lower panel of Figure 9, D% as plotted as a function of stimulation frequency for a constant supra-threshold current of stimulation. Consistently, as frequency of stimulation increases, D% decreases. These results indicate that frequency and current produce clear changes in how effectively the stimulus drives the activity of individual neurons. However, the shape of these curves may change depending on the constant frequency or current at which the current series or frequency series are obtained, respectively. We are currently obtaining this data in our neural recordings.

6. We are modeling our single neuron responses to understand the mechanism that underlies the modulation of neuron discharge with electrical stimulation frequency and current. Figure 10 displays the result of a single implementation of our model. To explore conceptually the connectivity between afferent fibers and second-order vestibular neurons, we implemented a simple integrate-and-fire scheme. The membrane potential of the vestibular unit is modeled using a first-order system and described by the following differential equation:

$$\dot{u} = -u - u_0 / \tau_m + I / C.$$

where u_0 is the resting potential of the unit, $\tau_m = RC$, the membrane time constant, with R and C denoting the resistance and capacitance, respectively, of the neuron. The activity of the afferent fibers is represented by a sequence of spikes (top traces in each panel of

Figure 10) firing at a constant rate with random drop-outs. The probability of drop-outs is varied to mimic different degrees of discharge regularity. Each afferent spike provides a current input source in the shape of an exponentially decaying step, which is reflected in the calculated potential after filtering through the dynamics of the membrane (Figure 10A). All the input currents from successive afferent spikes and emanating from different afferent fibers add linearly. For the purpose of this demonstration, the synaptic weights were set such that an afferent rate of 50 pps was insufficient to generate any post-synaptic spikes (Figure 10A), and such that three to four input spikes were needed upon temporal integration to yield an output spike at an input rate of 100 pps (Figure 10B).

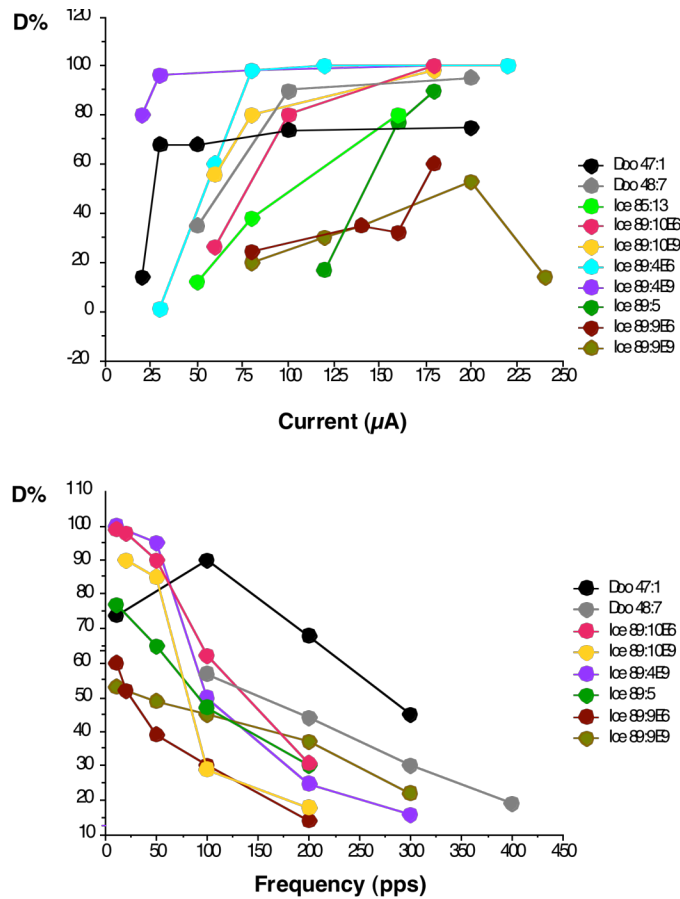


Figure 9: D% versus current or frequency of electrical stimulation for 10 neurons.

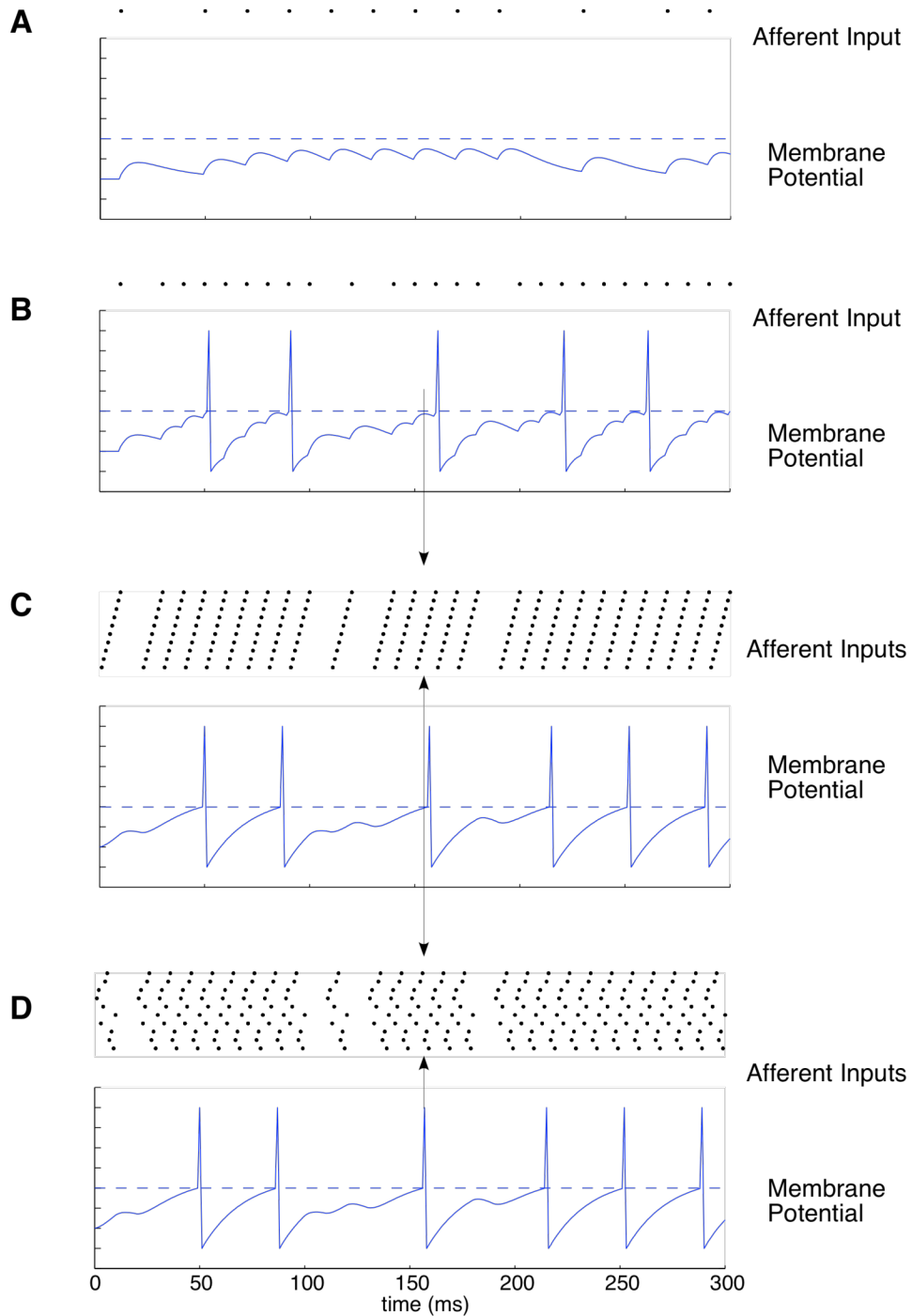


Figure 10. Simulated discharge of a presumed secondary vestibular neuron in response to afferent fiber input in a simple first order integrate and fire model.

The equations could also be used to describe the response of a unit with several parallel input streams. To facilitate comparison between different configurations, we adjusted the connectivity weights such that temporal synchrony of all input streams was equivalent to

a model with only a single input. In Figures 10C and 10D, we apply the same afferent input train as in Figure 10B (base rate of 100 pps) to a set of ten afferent fibers. In Figure 10C the trains are temporally staggered in a regular sequence, whereas in Figure 10D the order has been shuffled at random. In both cases, the output spike train has changed, demonstrating that subtle modifications in the structure of the model result in slightly different observed behaviors. Even this simple model can produce complex discharge behavior, and such subtle timing differences may produce significant effects for the interaction between inherent vestibular activity and spikes generated by electrical stimulation of the semi-circular canals. For example, in Figure 10, the timing of the spikes identified with arrows is changed very subtly by changing the alignment of the spike discharge. In Quarter 22, we intend to examine to what extent, and under what conditions, we can account for the results of our neural recordings without having to resort to more complex assumptions.

7. We submitted one meeting abstract, presented one paper, had one paper accepted for publication with minor revisions required, and finished another paper.

C. Phillips, S Bierer, C Kaneko, L Ling, K Nie, A Nowack, J Rubinstein, S Shepherd, J Phillips. Longitudinal Efficacy Of A Prosthesis Designed To Treat Pathological Nystagmus And Oscillopsia Resulting From Head Motion, ARVO, 2011, submitted

Steven M. Bierer, Leo Ling, Kaibao Nie, Jay T. Rubinstein, Trey Oxford, Amy L. Nowack, Chris R. Kaneko, Albert F. Fuchs, James O. Phillips Auditory outcomes following implantation and electrical stimulation of the semicircular canals. Hearing Research, Accepted with minor revisions.

James O. Phillips, Steven M. Bierer, Leo Ling, Kaibao Nie, and Jay T. Rubinstein, Real-time communication of head velocity and acceleration for an externally mounted vestibular prosthesis. EMBC 2011, presented, in press

Kaibao Nie, Steven M. Bierer, Leo Ling, Jay T. Rubinstein, and James O. Phillips Vestibular Neural Prostheses on Cochlear Implants: Design and Preliminary Results with Rhesus Monkeys Stimulated with Modulated Pulse Trains. IEEE BME, to be submitted in Quarter 22

Objectives for Quarter 22

- 1. In the next quarter we will continue recording longitudinal eye movement responses to electrical stimulation at different frequencies and current amplitudes.**
- 2. We will continue recording from the brainstem of our existing monkeys.** We are looking specifically for neurons that integrate amplitude modulated stimuli to produce a rate coded response. We will characterize D% performing current and frequency series as described above. We will also contrast the D% metric with other metrics of stimulus effectiveness, such as vector strength.

3. We will continue looking for vestibular afferent fibers, although these remain difficult to find and record in our preparation. Characterization of these afferents will provide a useful link in our analysis of the mechanisms underlying behaviorally effective electrical stimulation.

4. We will continue to characterize the sensitivity of recorded neurons to natural rotational stimuli at different rotational peak velocities to see whether there is a difference between neurons that are driven by electrical stimulation and those that are not.

5. We plan to test the newly developed bone anchored sensor array and processor.

6. We will continue to analyze and publish our data. We have two more manuscripts nearing completion, which we will submit in the next quarter.